Itinerant antiferromagnetism in infinite dimensional Kondo lattice

Shintaro Hoshino, Junya Otsuki, and Yoshio Kuramoto
Department of Physics, Tohoku University, Sendai 980-8578, Japan
(Received 29 December 2009; published 26 March 2010)

Highly accurate numerical results for single-particle spectrum and order parameter are obtained for the magnetically ordered Kondo lattice by means of the dynamical mean-field theory combined with the continuous-time quantum Monte Carlo method. Hybridized energy bands involving local spins are identified in the Néel state as a hallmark of itinerant antiferromagnetism. At the boundary of the reduced Brillouin zone, the twofold degeneracy remains in spite of the doubled unit cell. This degeneracy results if the molecular field felt by localized spins has identical magnitude and reversed direction with that of conduction electrons. The persistent Kondo effect is responsible for the behavior. The antiferromagnetic quantum transition occurs inside the itinerant regime and does not accompany the itinerant-localized transition.

DOI: 10.1103/PhysRevB.81.113108 PACS number(s): 71.27.+a, 75.20.Hr, 64.70.Tg

The distinction between itinerant and localized characters of strongly correlated electrons has been one of the most fundamental issues in condensed-matter physics. The Kondo effect plays a central role in this problem because even a localized spin may acquire itinerant character by coupling with conduction electrons, and may form a Fermi liquid. Some of recent experiments suggest that quantum phase transition between magnetic and paramagnetic ground states accompanies a change between localized and itinerant characters of electrons, with a non-Fermi-liquid behavior in the vicinity of the transition.[1] Another experiment using the de Haas-van Alphen effect has probed the change in the Fermi surface as the external pressure drives such systems as $CeIn_3$ and $CeRhIn_5$ across the magnetic transition.[2] On the other hand, recent photoemission experiment for $CeRu_2Si_2$ and $CeRu_2Si_{2-x}Ge_x$ indicates that the Fermi surfaces of both are essentially the same, which involve f electrons and are referred to as the large Fermi surface. The experiment is performed at temperatures above the Néel transition of $CeRu_2Si_{2-x}Ge_x$,[3] while $CeRu_2Si_2$ remains paramagnetic down at least to 0.1 K. Thus, the antiferromagnetism in $CeRu_2Si_{2-x}Ge_x$ seems to be itinerant. Consistent understanding of this variety of phenomena is highly desirable, but is still lacking.

In this Brief Report, we report on finite temperature results that provide understanding of how the magnetic order is related to the change from itinerant to localized characters of electrons. It is obvious that the issue is not restricted to a particular compound. Hence, we work with the Kondo lattice model (KLM) since the KLM is the simplest system that is capable of describing both itinerant and localized characters of electrons. The KLM is given by

$$\mathcal{H} = \sum_{k\sigma} \varepsilon_k c^\dagger_{k\sigma} c_{k\sigma} + 2J \sum_i \boldsymbol{S}_i \cdot \boldsymbol{s}_{ci}, \tag{1}$$

where the first term represents the kinetic energy of conduction electrons, $\boldsymbol{S}_i$ is the localized spin at site i, and $\boldsymbol{s}_{ci} = \frac{1}{2}\Sigma_{\alpha\beta} c^\dagger_{i\alpha} \boldsymbol{\sigma}_{\alpha\beta} c_{i\beta}$ denotes the conduction-electron spin at the same site. The competition between the Ruderman-Kittel-Kasuya-Yosida (RKKY) interaction and the Kondo effect determines the phase diagram.[4]

The ordered phase in the KLM has been investigated beyond the mean-field theory in one- (Refs. 5 and 6) and two- (Refs. 7–11) dimensional systems. We approach the KLM from infinite dimensions using the dynamical mean-field theory (DMFT) to allow for the Néel state at finite temperatures. We use the continuous-time quantum Monte Carlo method (CT-QMC) (Refs. 12–14) as the impurity solver and focus on the case of unit number $n_c = 1$ of conduction electrons per site. In contrast with the metallic antiferromagnetism with $n_c \neq 1$, where an incommensurate order may exist, we can safely assume the simple staggered order because of the nesting condition for the conduction band in the hypercubic lattice. Hence, the results in this Brief Report are exact in infinite dimensions except for statistical errors.

As the half-filled limit is approached from $n_c \neq 1$, the large Fermi surface tends to the zone boundary of the paramagnetic phase, while the small Fermi surface involves half of the Brillouin zone volume. Provided that the ground state has no discontinuity in the zero-doping limit, the limiting location of the Fermi surface should be reflected in the location of the energy gap in the half-filled case. In the localized antiferromagnetism, the gap opens at the boundary of the new Brillouin zone since conduction electrons feel the staggered internal field. In itinerant magnetism, on the other hand, we show in this Brief Report that the energy gap is located in the center of the new Brillouin zone. The zone-center location is due to the emergence of energy bands of magnetic electrons. Hence, the location of the energy gap distinguishes between itinerant and localized behaviors. Note that such a distinction does not apply to the single band model such as the Hubbard model where the energy gap in the half-filled limit always occurs in the boundary of the Brillouin zone. In this case the character of electrons changes continuously from the itinerant limit to the localized one, as the Coulomb repulsion increases relative to the band width.

We take the bare density of states

$$\rho_c(\omega) = \sqrt{2/\pi}\, \exp(-2\omega^2), \tag{2}$$

which corresponds to an infinite dimensional hypercubic lattice. We have taken the bandwidth $D=1$ as the unit of energy.

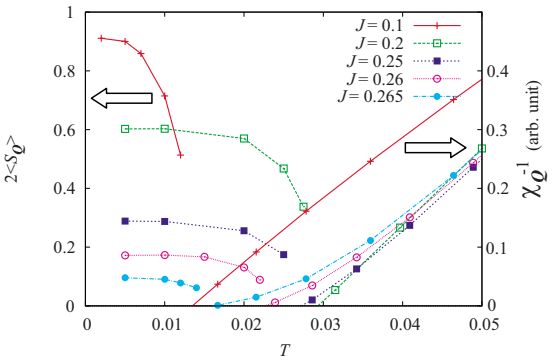

FIG. 1. (Color online) Staggered spin polarization $2\langle S^z_{\boldsymbol{Q}}\rangle$ (left scale) as a function of temperature for different values of J. Also shown is the inverse staggered susceptibility $\chi^{-1}_{\boldsymbol{Q}}$ (right scale), which goes to zero at $T_{\rm N}$.

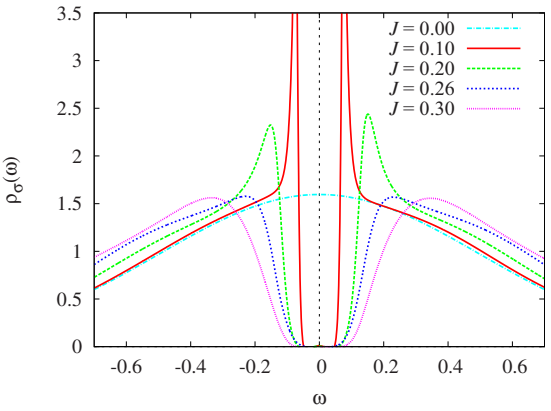

FIG. 2. (Color online) J dependence of the density of states for the conduction electron and with $T\sim 0$.

For the Gaussian density of states, the Kondo temperature $T_{\rm K}$ is defined by

$$\rho_{\rm c}(0)T_{\rm K} = \frac{e^{-\gamma/2}}{\sqrt{\pi}}\exp\left(-\frac{1}{2\rho_{\rm c}(0)J}\right), \tag{3}$$

where $e^{-\gamma/2}/\sqrt{\pi}\sim 0.42$ with $\gamma\simeq 0.577$ being the Euler constant. This expression of $T_{\rm K}$ corresponds to divergence of effective exchange in the lowest-order scaling equation.

The hypercubic lattice has the nesting property with the wave vector $\boldsymbol{Q}=(\pi,\pi,\ldots)$ at half filling, which favors the staggered order. In the two-sublattice formalism, the Green's function $\boldsymbol{G}_{\boldsymbol{k}\sigma}(z)$ of conduction electrons is a 2×2 matrix where z is a complex energy, and a wave vector $\boldsymbol{k}$ belongs to the reduced Brillouin zone.[15] In the DMFT, the wave vector enters only through $\varepsilon_{\boldsymbol{k}}$. Therefore, we introduce the notation $\kappa=\varepsilon_{\boldsymbol{k}}$ and regard κ as if it represents a wave number. The spectral function $A_\sigma(\kappa,\omega)$ can be calculated from the matrix Green's function $\boldsymbol{G}_\sigma(\kappa,z)$ as

$$A_\sigma(\kappa,\omega) = -\,\mathrm{Im}[\mathrm{Tr}\,\boldsymbol{G}_\sigma(\kappa,\omega+i\delta)]/\pi. \tag{4}$$

Then the renormalized density of states $\rho_\sigma(\omega)$ is given by $\rho_\sigma(\omega)=2N^{-1}\Sigma_{\boldsymbol{k}}A_\sigma(\varepsilon_{\boldsymbol{k}},\omega)$, where the summation runs over the reduced Brillouin zone with $N/2$ points. In the paramagnetic state, the reduced number of $\boldsymbol{k}$ is compensated by the trace over $\boldsymbol{G}_{\boldsymbol{k}\sigma}(z)$ to give the same $\rho_\sigma(\omega)$ as derived by the use of the original Brillouin zone. Even in the Néel state, $\rho_\sigma(\omega)$ does not depend on σ because of the summation over sublattices.

Let us first discuss the magnitude of the staggered moment given by $2\langle S^z_{\boldsymbol{Q}}\rangle=\langle S^z_{\rm A}\rangle-\langle S^z_{\rm B}\rangle$. The RKKY interaction is responsible for the effective magnetic field, which is determined self-consistently as in the standard mean-field theory. Figure 1 shows the temperature dependence of the staggered moment, which should vanish at the Néel temperature $T_{\rm N}$. On the other hand, the staggered magnetic susceptibility $\chi_{\boldsymbol{Q}}$ in the paramagnetic state should diverge as the temperature is lowered toward $T_{\rm N}$. Hence, we also plot $\chi^{-1}_{\boldsymbol{Q}}$ calculated in Ref. 4. It is found that the estimates of $T_{\rm N}$ by $\langle S^z_{\boldsymbol{Q}}\rangle$ and $\chi^{-1}_{\boldsymbol{Q}}$ are consistent with each other. However, the calculation of $\langle S^z_{\boldsymbol{Q}}\rangle$ becomes increasingly difficult as T is approached to $T_{\rm N}$. The results shown in Fig. 1 are restricted to the temperature range where we could obtain reliable values. With $J=0.1$, the localized spins are almost fully polarized in the ground state. The temperature dependence can be fitted very well by the mean-field formula, provided the saturated magnetization at $T=0$ is given. As J increases, $\langle S^z_{\boldsymbol{Q}}\rangle$ decreases by the Kondo effect, which eventually suppresses the antiferromagnetism at $J=J_{\rm c}\simeq 0.27$ down to $T=0$. With $J\gtrsim 0.2$, the mean-field theory does no longer provide a good fit for the temperature dependence.

We next discuss the density of states near $T=0$, which is derived using the Padé approximation for analytical continuation from imaginary Matsubara frequencies $i\varepsilon_n$ to the real ones. Since the Monte Carlo data are obtained accurately in the imaginary time domain, the Padé approximation works well in the CT-QMC method.[14] Figure 2 shows $\rho_\sigma(\omega)$ for different values of J near the ground state. Namely, we take the temperature where the density of states does not vary much when T decreases further. For example, we take $T=0.01$ for $J=0.3$, but $T=0.002$ for $J=0.1$. The present method has no difficulty to go to such low temperatures with high accuracy. In the case of $J=0.3$ with the paramagnetic ground state, the density of states has a gap caused by the Kondo effect. The state is often called the Kondo insulator. In the case of $J=0.26$, the ground state is antiferromagnetic as seen from Fig. 1. The density of states in the ordered phase is almost the same as that with $J=0.3$. Namely, the density of states does not depend much on whether the ground state is paramagnetic or antiferromagnetic as long as J is close to the critical value $J_{\rm c}$.

When J is smaller, sharp peaks develop at both edges of the gap. The origin is understood as follows: putting the self-energy of conduction electrons as the staggered potential $\pm h$ by the Néel order, we obtain

$$\mathrm{Tr}\,\boldsymbol{G}_\sigma(\kappa,z) = (z+\sqrt{\kappa^2+h^2})^{-1} + (z-\sqrt{\kappa^2+h^2})^{-1}. \tag{5}$$

Then the density of states is given by

$$\rho_\sigma(\omega) = \frac{2|\omega|}{\sqrt{\omega^2-h^2}}\rho_{\rm c}(\sqrt{\omega^2-h^2}), \tag{6}$$

with a square-root divergence at both edges $\omega=\pm h$. For $\omega^2<h^2$, we obtain $\rho_\sigma(\omega)=0$. This form of $\rho_\sigma(\omega)$ roughly

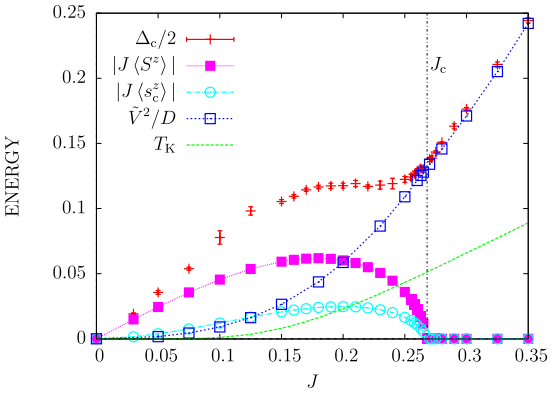

FIG. 3. (Color online) J dependence of the energy gap $\Delta_c/2$. For comparison, also plotted are $J\langle S^z\rangle$, $J\langle s_c^z\rangle$; S^z and s_c^z are the localized and conduction spins at a local site, respectively. $\tilde{V}^2/D$ represents the effective hybridization to be explained later, and T_K is the Kondo temperature defined by Eq. (3).

explains the peak structure with $J=0.1$ in Fig. 2. In the numerical result, the residual Kondo effect actually suppresses the divergence in $\rho_\sigma(\omega)$.

On the other hand, the density of states for larger J does not show a clear threshold. The Gaussian tail in the bare density of states $\rho_c(\omega)$ causes a tiny but finite magnitude of $\rho_\sigma(\omega)$ within the apparent energy gap. Therefore, we introduce the characteristic value Δ_c of the energy gap as giving the half-maximum value of the peak in the density of states. Figure 3 shows $\Delta_c/2$ as a function of J. The error bars have been estimated from five bins of data. It is clear that Δ_c changes continuously at $J=J_c$. This shows that both the Kondo effect and the staggered internal field are contributing to Δ_c. For $J \lesssim 0.1$, on the other hand, $\Delta_c/2$ is almost proportional to J. This behavior shows that the gap is mainly determined by the staggered field $J\langle S^z\rangle$ as shown also in Fig. 3.

The details of the itinerancy are seen in the single-particle spectral function $A_\sigma(\kappa,\omega)$. Figure 4 shows the spectrum in the case $J=0.2$ where the Kondo effect is significant. In both paramagnetic and ordered phases, the spectrum consists of four bands in the reduced Brillouin zone. In the paramagnetic phase shown in the left panel, the new bands are ascribed to "hybridization bands" caused by the Kondo effect.[16] We note that there is no real hybridization between the f and conduction electrons because the f electron does not have the charge degrees of freedom in the KLM. In the Brillouin zone of the paramagnetic state, the energy gap is indirect from the zone boundary to the zone center, both of

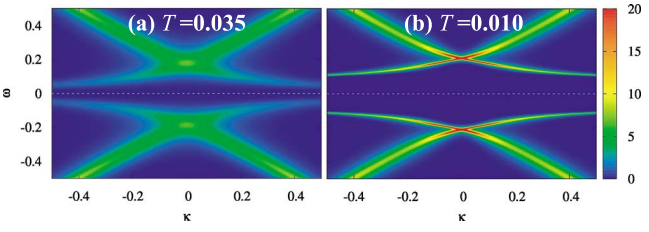

FIG. 4. (Color online) Single-particle spectrum with $J=0.2$ in (a) paramagnetic phase at $T=0.035$ and (b) antiferromagnetic phase at $T=0.010$.

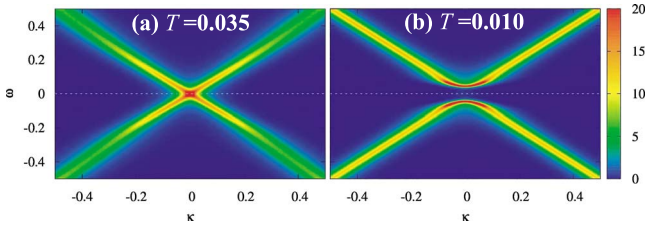

FIG. 5. (Color online) $A_\sigma(\kappa,\omega)$ with ferromagnetic interaction $J=-0.2$ in (a) paramagnetic phase at $T=0.035$ and (b) antiferromagnetic phase at $T=0.010$.

which correspond to $\kappa \to \pm\infty$ in Fig. 4. In the right panel of Fig. 4(b), these hybridization bands are clearly seen even in the antiferromagnetic phase. Hence, we classify the antiferromagnetism in this regime as itinerant.

Let us now present the spectrum in the ferromagnetic KLM for comparison, where each site forms $S=1$ state with antiferromagnetic intersite interaction. The Kondo effect is absent in the case of $J<0$. We can apply the CT-QMC method also to ferromagnetic J as noted in Ref. 17. Figure 5 shows the spectrum with the same T as in Fig. 4. In the paramagnetic state shown in Fig. 5(a), the spectrum is almost the same as the original conduction band. On the other hand, in the antiferromagnetic phase shown in Fig. 5(b), the spectrum shows the clear gap structure. These behaviors are explained well by Eq. (5) with $h=0$ in Fig. 5(a), while $h\neq 0$ in Fig. 5(b). In the case of ferromagnetic J, the number of bands is two in contrast to the case with $J>0$ with four bands.

Thus, the itinerant or localized behavior can be distinguished by the number of energy bands in the reduced Brillouin zone. Moreover, the location of the energy gap is at the zone boundary in the localized case, but at the zone center in the itinerant case. Note that $\kappa=\pm\infty$ correspond to the lower and upper edges of the conduction band in infinite dimensions. Both edges come to the center in the reduced Brillouin zone.

We note another characteristic feature in Fig. 4(b) that the degeneracy at $\kappa=0$ remains in the antiferromagnetic phase. A toy model helps one to understand the origin of the degeneracy. Let us consider a noninteracting periodic Anderson model under the staggered field as

$$\mathcal{H}_{\mathrm{PAM}} = \sum_{k\sigma} \varepsilon_k c_{k\sigma}^\dagger c_{k\sigma} + V\sum_{i\sigma}(f_{i\sigma}^\dagger c_{i\sigma} + \mathrm{H.c.}) + 2\sum_i (h_i s_{ci}^z + H_i S_i^z), \tag{7}$$

where $f_{i\sigma}$ ($f_{i\sigma}^\dagger$) is the annihilation (creation) operator of an f electron at the i site with the hybridization V. The staggered fields represent the molecular field associated with the antiferromagnetism. Then we choose $h_i=\pm h$ and $H_i=\pm H$, where the A (B) sublattice has the positive (negative) sign.

There are four branches associated with c and f degrees of freedom for the electrons, as well as the presence of A and B sublattices. At $\kappa=0$, we obtain the energies

$$E(\kappa=0) = \pm\frac{1}{2}[(h+H) \pm \sqrt{(h-H)^2+4V^2}]. \tag{8}$$

If the relation $h=-H$ holds, $E(\kappa=0)$ has only two distinct values both of which are doubly degenerate. We interpret the

degeneracy in Fig. 4(b) as caused by the relation $h=-H$ for the molecular field. We call such a situation "quasilocal compensation." Note that the magnitudes of the polarization for the conduction spin $J\langle s_c^z\rangle$ and localized spin $J\langle S^z\rangle$ are much different as shown in Fig. 3. Hence, the actual energy level is determined not by the local internal field, but by a long-range field involving remote conduction electrons. The compensation is reminiscent of the spatially extended Kondo singlet with small J.

Let us identify the energy scale in the Néel state from the self-energy. For sublattice $\alpha=\pm 1$ and spin $\sigma=\pm 1$, $\Sigma_{\alpha\sigma}(z)$ is expanded as

$$\Sigma_{\alpha\sigma}(z) = \alpha\sigma h + \frac{\tilde{V}^2}{z} + O\left(\frac{1}{z^2}\right), \tag{9}$$

where $\tilde{V}$ is the effective hybridization. The coefficient $\tilde{V}^2$ of $1/z$ corresponds to the jump at $\tau=0$ in the imaginary time domain. We extract numerically the coefficient $\tilde{V}^2$ of $1/i\varepsilon_n$ in the self-energy. Figure 3 shows the result for $\tilde{V}^2/D(=\tilde{V}^2)$ as a function of J. Note that the indirect energy gap in the toy model (7) is given by V^2/D. The agreement between $\tilde{V}^2/D$ and $\Delta_c/2$ in the paramagnetic phase is excellent. However, this consistency should not be taken too seriously because Δ_c depends on the definition of the gap. We emphasize that $\tilde{V}^2/D$ shows no anomaly across the phase transition to the antiferromagnetic phase. It also shows good proportionality to the Kondo temperature as $\tilde{V}^2/D \simeq 2.6T_K$.

In the region $0<J\lesssim 0.1$, the Néel temperature T_N is much larger than T_K as seen from Figs. 1 and 3. The electronic state at the transition has a localized character since the Kondo effect is negligible at T_N. Namely, there is no hybridized band, and the energy gap occurs at the boundary of the reduced Brillouin zone. However, we have checked that two almost flat bands appear newly below T_K even with $J=0.05$. Hence, the crossover from the localized behavior to the itinerant one occurs inside the Néel ordered state.

In summary, we have derived single-particle spectrum and the temperature-dependent order parameter in the infinite dimensional KLM allowing for the Néel order. The high numerical accuracy has made it possible to find the quasilocal compensation between the conduction and localized spins indicating the persistent tendency toward the Kondo singlet at each site. The effective hybridization energy has no anomaly across the quantum phase transition, and it scales well with the impurity Kondo temperature T_K. Hence, the quantum transition into antiferromagnetism occurs within the itinerant regime and does not involve itinerant-localized transition.

[1] P. Gegenwart, Q. Si, and F. Steglich, Nat. Phys. **4**, 186 (2008).
[2] R. Settai, T. Takeuchi, and Y. Onuki, J. Phys. Soc. Jpn. **76**, 051003 (2007).
[3] T. Okane *et al.*, Phys. Rev. Lett. **102**, 216401 (2009).
[4] J. Otsuki, H. Kusunose, and Y. Kuramoto, J. Phys. Soc. Jpn. **78**, 034719 (2009).
[5] H. Tsunetsugu, M. Sigrist, and K. Ueda, Rev. Mod. Phys. **69**, 809 (1997).
[6] N. Shibata and H. Tsunetsugu, J. Phys. Soc. Jpn. **68**, 744 (1999).
[7] F. F. Assaad, Phys. Rev. Lett. **83**, 796 (1999).
[8] S. Capponi and F. F. Assaad, Phys. Rev. B **63**, 155114 (2001).
[9] H. Watanabe and M. Ogata, Phys. Rev. Lett. **99**, 136401 (2007).
[10] L. C. Martin and F. F. Assaad, Phys. Rev. Lett. **101**, 066404 (2008).
[11] N. Lanatà, P. Barone, and M. Fabrizio, Phys. Rev. B **78**, 155127 (2008).
[12] A. N. Rubtsov, V. V. Savkin, and A. I. Lichtenstein, Phys. Rev. B **72**, 035122 (2005).
[13] P. Werner and A. J. Millis, Phys. Rev. B **74**, 155107 (2006).
[14] J. Otsuki, H. Kusunose, P. Werner, and Y. Kuramoto, J. Phys. Soc. Jpn. **76**, 114707 (2007).
[15] A. Georges, G. Kotliar, W. Krauth, and M. J. Rozenberg, Rev. Mod. Phys. **68**, 13 (1996).
[16] J. Otsuki, H. Kusunose, and Y. Kuramoto, Phys. Rev. Lett. **102**, 017202 (2009).
[17] S. Hoshino, J. Otsuki, and Y. Kuramoto, J. Phys. Soc. Jpn. **78**, 074719 (2009).